Progress In Electromagnetics Research, Vol. 145, 203–212, 2014

A General Method for Designing a Radome to Enhance the Scanning Angle of a Phased Array Antenna

Fei Sun[1, 2], Shuai Zhang[1, 2], and Sailing He[1, 2, *]

Abstract—We propose a general method to design an arbitrarily shaped radome which can extend the scanning angle of a phased array antenna through finite embedded transformation (FET). The main advantage of our method is that the relationship between the incident angle and steered output angle of the radome can be designed in advance (e.g., a linear relation can be achieved). Unlike a traditional FET, which is often applied onto a slab region, we first apply FET onto an arbitrarily shaped region to bestow the desired radome with an arbitrary shape. Two specific examples have been given to demonstrate our method. Numerical simulations show good performance of our radome.

1. INTRODUCTION

Phased array antennae (PAA) have been widely used in mobile communications, satellite broadcasting, space probe communication, radar system and radio astronomy [1]. Most available phased array antenna systems can achieve an electromagnetic beam scanning from $-60°$ to $60°$ [1]. However, as the angle of scanned beam increases, the performance of the PAA decreases (e.g., the directivity degrades and side lobes increase). Many methods have been proposed to increase the scanning angle of a PAA. One way is the utilization of mechanical augmentations, which sacrifices the main advantage of a PAA (electronically scanning without the mechanical time delay). A good method is to extend the scanning angle of a PAA by using a specially designed radome, which can steer the beam produced by PAA to a larger angle [2, 3]. In 2011, Lam et al., have proposed a Bucky-ball NIM lens that can steer beams produced by a PAA to the horizon [3]. The proposed Bucky-ball NIM lens shows good performance numerically and experimentally. However this Bucky-ball NIM lens still has some disadvantages. Firstly, the designing process of this Bucky-ball NIM lens is very complex. It requires an optimization process (over 8000 simulations have been run) to determine an initial 2D structure and then extend this structure to a 3D one. After that, it requires a conformal mapping technique that transforms the radome with an elliptical cross section to one with a circular cross section or a Bucky-ball structure. Secondly, the relationship between the input beam produced by a PAA and the output beam steered by the radome is not linear. In fact, this method cannot determine the specific relation between the input angle and the output angle. It is simply an optimization process to ensure that when the input beam is $60°$, the output beam can be maximally steered (e.g., steered to the horizon). However in many practical applications, it often needs a linear relationship between the input beam and the steered output beam. In this paper, we will introduce a general method to design a novel radome that can overcome the above drawbacks and lead a new way to design an arbitrarily shaped radome for the PAA.

Our method is based on transformation optics (TO), which has been widely used to design invisible cloaks [4, 5], perfect lenses [6], DC magnetic field lenses/concentrators [7–10], etc. [11]. We can divide

Received 7 March 2014, Accepted 21 March 2014, Scheduled 24 March 2014

* Corresponding author: Sailing He (sailing@kth.se).

[1] Centre for Optical and Electromagnetic Research, Zhejiang Provincial Key Laboratory for Sensing Technologies, JORCEP, East Building #5, Zijingang Campus, Zhejiang University, Hangzhou 310058, China. [2] Department of Electromagnetic Engineering, School of Electrical Engineering, Royal Institute of Technology (KTH), Stockholm S-100 44, Sweden.

the devices designed by TO into two kinds: one kind has an enclosed structure that produces a local phenomenon and does not influence the electromagnetic wave outside the device (e.g., invisible cloak [4, 5], electromagnetic wave concentrators [12], field rotators [13], invisible sphere [4], etc.). Note that people choose the identical transformation at the outer boundary of this kind of device, which is why such devices can only produce a local influence on electromagnetic waves. Another kind of device is designed by a finite embedded transformation (FET) [14], which can produce a non-local phenomenon and influence the far field (e.g., beam shifter [14], beam splitter [14], beam compressor [15], polarization controller [16], etc.). Traditionally the device designed by FET is often a slab shaped device with an identical transformation at the input plane and a discontinuous transformation at the output plane, which is the key point to cause desired influences of the electromagnetic wave after it passes through the devices.

In this paper, we will apply an FET onto an arbitrary shell region to design a radome that can extend the scanning angle of a PAA. Compared with the previous method [2, 3], our method has the following advantages: firstly, the relationship between the incident beam produced by a PAA and the output beam steered by our radome can be designed in advance (e.g., a linear relationship can be achieved); secondly, the design process of our method is very simple and does not need any optimization; and thirdly, the shape of the radome can be designed arbitrarily which can be chosen according to the practical application.

2. METHOD

TO can build up a relationship between two spaces: one is a virtual space (reference space) and the other is the real space. By using a special coordinate transformation, we can get the materials (referred as the transformed medium) with the desired function in the real space. These transformed media can perform the same coordinate transformation to the electromagnetic wave from the reference space to the real space. Note that the detail of TO can be found in Ref. [4]. In this paper, the quantities with or without primes correspond to the quantities in the real or reference space, respectively. For simplicity, we first consider a 2D case (the whole structure is infinitely long along the z' axis). As shown in Fig. 1, a

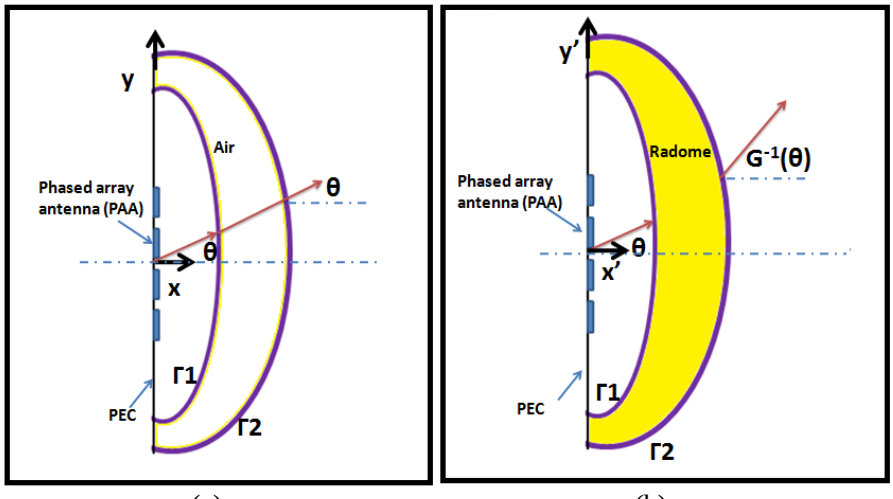

Figure 1. The transformation relationship between (a) the reference space and (b) the real space. Γ_1 and Γ_2 (purple lines) represent two boundaries of arbitrary shape, which are the same in both spaces. Γ_1 and Γ_2 are symmetrical to the x (also x')-axis and intersect with the y (also y')-axis. (a) The reference space is a half space ($x > 0$) filled with air. A PAA is located on a PEC ground at $x = 0$. A beam with propagating angle θ is produced by the PAA both in the reference space and the real space. (b) The real space is still a half space ($x' > 0$); except for the transformed medium indicated by the yellow region enclosed by Γ_1 and Γ_2 (our radome), other regions are still free space.

PAA is located on a PEC plane both in the reference space and the real space. We only need to consider a half space ($x' > 0$) problem here. The reference space now is a half space ($x > 0$) filled with air (see Fig. 1(a)). We divide this half space into three regions by introducing two arbitrary curves Γ_1 and Γ_2, which are both symmetrical about the x-axis and intersect with the PEC plane $x = 0$. We apply an identical transformation to the regions, excluding the region enclosed by Γ_1 and Γ_2. This means that, except for the region enclosed by Γ_1 and Γ_2, the other regions are still free space in the real space. The only transformed region is the region enclosed by Γ_1 and Γ_2, which stands for our device (the yellow region in Fig. 1(b)). We can choose the following transformation onto the region between Γ_1 and Γ_2:

$$\begin{aligned} r &= r' \\ \theta &= f\left(r'\left(x', y'\right), \theta'\left(x', y'\right)\right) \\ z &= z' \end{aligned} \tag{1}$$

where continuous function f satisfies

$$f|_{\Gamma_1} = \theta'; \quad f|_{\Gamma_2} = G(\theta') \tag{2}$$

Γ_1 and Γ_2 represent the inner and outer boundaries of our radome. The above transformation means that we choose an identical transformation $\theta' = \theta$ at the input surface of our device Γ_1. Note that θ is the angle of the incident beam both in the reference space and the real space. As the reference space is the free space, the light beam will keep propagating with same angle θ in the reference space (see Fig. 1(a)). Once the transformation function f is continuous from Γ_1 to Γ_2, θ' will gradually change from θ to $G^{-1}(\theta)$. Note that the output angle also equates the incident angle in the reference space; therefore we obtain the relation between the input angle and output angle in the real space:

$$\theta_{output} = G^{-1}\left(\theta_{input}\right) \tag{3}$$

We should note that this result shows the main advantage of our method: we can determine the relation between the incident angle and the steered angle in advance. Other methods cannot achieve this [2, 3]. In many applications, a linear relationship between the input angle and output angle is often desirable. Now we will provide a simple example that presents a linear relationship between the incident and output angles. To introduce our idea analytically, we can first assume that Γ_1 and Γ_2 are both cylindrical surfaces with radius R_1 and R_2, respectively. Later we will give a general method in which Γ_1 and Γ_2 can be of arbitrary shape. We choose f as the following form:

$$f\left(r', \theta'\right) = \theta' + \frac{R_1 - r'}{R_2 - R_1}\left[(1 - M)\theta' + M\theta_0\right] \tag{4}$$

Note that by choosing such a transformation function f in Eq. (4), we have $G(\theta') = M\theta' - M\theta_0$, i.e.,

$$\theta_{output} = G^{-1}(\theta_{input}) = \frac{1}{M}\theta_{input} + \theta_0 \tag{5}$$

It means that such a radome can produce a linear relationship between the incident angle and the output angle. We can determine the corresponding transformed medium by using transformation optics [4, 5]:

$$\bar{\bar{\varepsilon}} = \bar{\bar{\mu}} = \begin{bmatrix} m_2 & -m_1 & 0 \\ -m_1 & \frac{1}{m_2}\left(1 + m_1^2\right) & 0 \\ 0 & 0 & m_2 \end{bmatrix} \tag{6}$$

with

$$m_1 = -\frac{r'}{R_2 - R_1}\left[(1 - M)\theta' + M\theta_0\right]; \quad m_2 = 1 + \frac{R_1 - r'}{R_2 - R_1}(1 - M) \tag{7}$$

Note that the permeability and permeability tensors in Eq. (6) are expressed in a cylindrical coordinate system. r, θ, z are principle value orientations of the tensor. In simulation, we need to express it in the Cartesian coordinate system. We rewrite Eq. (6) in the Cartesian coordinate system as:

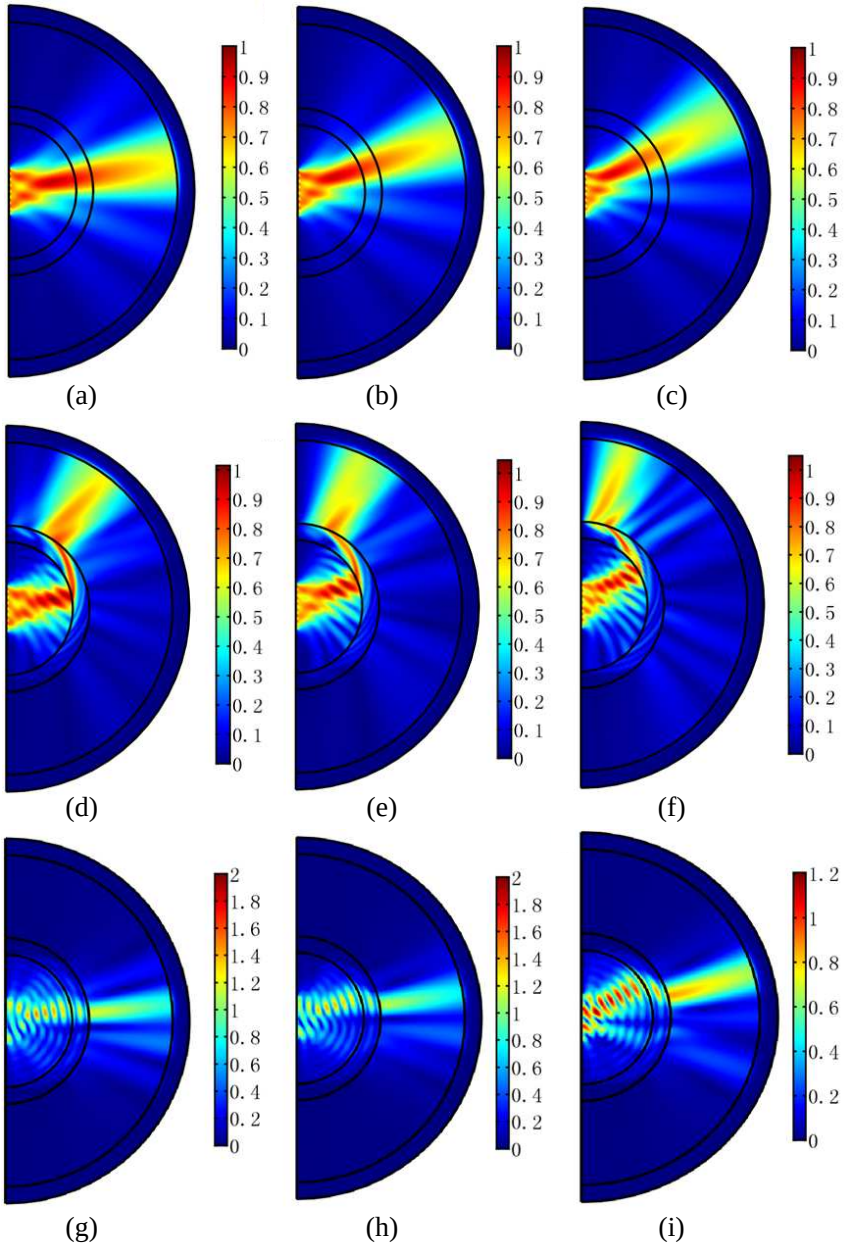

Figure 2. 2D FEM simulation results: the amplitude of the electric field distribution. The TE model (where the electric field is orthogonal to the x'-y' plane) is chosen here. Now the shape of our radome is a cylindrical shell with inner radius $R_1 = 4\lambda_0$ and outer radius $R_2 = 5\lambda_0$. The whole simulation domain is in a half circle with radius $11\lambda_0$, and the perfectly matched layer with thickness λ_0 is chosen as the exterior boundary. An 8×1 PAA, which is the array of line segments with equal length $0.25\lambda_0$ and center-to-center spacing $d = 0.35\lambda_0$, is set along the PEC ground (y' axis). (a), (b) and (c) Beams with angles 10°, 20° and 30°, respectively, are produced by the PAA (without our radome). (d), (e) and (f) We set a radome with $M = 1$ and $\theta_0 = 45°$ (an angle shifter) in Eq. (4) after the PAA in (a), (b) and (c) respectively. As we can see, the incident beams with angles 10°, 20° and 30° are steered to 55°, 65° and 75° respectively by a fixed angle 45° shift. (g), (h) and (i) We set a radome with $M = 2$ and $\theta_0 = 0°$ (an angle compressor) in Eq. (4) after the PAA in (a), (b) and (c) respectively. In this case, although the main angle of the output beam is transformed to 5°, 10° and 15° respectively, the whole beam is also compressed. These features can be explained by Eq. (5).

$$\bar{\bar{\varepsilon}}=\bar{\bar{\mu}}=\begin{bmatrix} m_2\dfrac{x'^2}{x'^2+y'^2}+\dfrac{(1+m_1^2)}{m_2}\dfrac{y'^2}{x'^2+y'^2}+2m_1\dfrac{x'y'}{x'^2+y'^2} & \left(m_2-\dfrac{(1+m_1^2)}{m_2}\right)\dfrac{x'y'}{x'^2+y'^2}-m_1\left(\dfrac{x'^2}{x'^2+y'^2}-\dfrac{y'^2}{x'^2+y'^2}\right) & 0 \\ \left(m_2-\dfrac{(1+m_1^2)}{m_2}\right)\dfrac{x'y'}{x'^2+y'^2}-m_1\left(\dfrac{x'^2}{x'^2+y'^2}-\dfrac{y'^2}{x'^2+y'^2}\right) & m_2\sin^2\phi+\dfrac{(1+m_1^2)}{m_2}\dfrac{x'^2}{x'^2+y'^2}-2m_1\dfrac{x'y'}{x'^2+y'^2} & 0 \\ 0 & 0 & m_2 \end{bmatrix} \quad (8)$$

Next we will use the finite element method (FEM) to verify the performance of the device [17]. Due to the basic principle that a PAA can be treated as a result of a multi-beam interference, we can simply set some line sources with fixed phase delay to mimic PAA. For a given direction of the scanning beam (θ, ϕ), the phase delay for an element in the array can be given as [3]:

$$\psi_m = -k_0\left(\sin\theta\cos\varphi x_m + \sin\theta\sin\varphi y_m\right) \quad (9)$$

where $k_0 = 2\pi/\lambda_0$ is the free space wave number and (x_m, y_m) is the coordinate of a particular element in the PAA. Here λ_0 is the wavelength in the free space. For a 2D case, we assume that the PAA is located along the y-axis, and therefore the above equation can be reduced to:

$$\psi_m = -k_0\sin\theta y_m \quad (10)$$

In our simulation, all lengths have been normalized by the free space wavelength. An 8×1 PAA is utilized, which consists of 8 line segments with equal lengths of $0.25\lambda_0$ (each line segment behaves like the opening of a dielectric filled horn antenna) and center-to-center spacing of $d = 0.35\lambda_0$. This PAA produces an initial incident angle from 10° to 30°, as shown in Figs. 2(a)–(c). We can design the angle of the output beam by either shifting by a fixed angle θ_0 (see Figs. 2(d)–(f) where $\theta_0 = 45°$ for an angle shifter) or multiplying by a fixed factor $1/M$ (see Figs. 2(g)–(i) where $M = 2$ for an angle compressor). If $M < 1$, the output scan angle can be linearly enlarged by $1/M$ times the input scan angle. These simulation results verify the performance of our radome and confirm that the relationship between the incident beam and the output beam can be designed in advance. The normalized electric far fields are given in Fig. 3. In Fig. 3(a), we compare the normalized electric far field patterns between beams of angle 65° produced by a PAA and produced by our radome after the same PAA (but with a different value for the phase delay). Note that here we choose a PAA with a relatively flat far-field pattern for a single unit to ensure that this PAA can produce an output beam with an angle of 65°. In practice, it is challenging for the PAA to produce a beam with an angle larger than 60° due to the surface-wave-like mode [19], the impedance matching variation in different scanning angles, and the limitation of the radiation pattern of each array element. Fig. 3(a) shows that we can obtain a beam with an angle larger than 60° in the far field by setting our radome after a beam with an angle far smaller than 60° (e.g., 20°) produced by a PAA. We can also observe from Fig. 3(a) that for a scanning angle larger than 60°, the beam width and side lobe level with the proposed radome are much better than those of the conventional PAA.

If we choose $\theta_0 = 0$ and $M > 1$, our radome can perform as a beam angle compressor which can compress both the central angle and beam width (see Figs. 2(g)–(i)). Note that the angle width of the output beam has only been reduced in some distance regions (e.g., $5\lambda_0$ to $10\lambda_0$ after the PAA). However, once the compressed beam propagates to the far field, it diverges due to the diffraction (see Fig. 3(b)). We should also mention that if we choose $\theta_0 \neq 0$ and $M > 1$ at the same time (see Figs. 3(c)–(d)), we can obtain a single radome with multiple functions: one function is compression of the beam width produced by the PAA; the other function is extending the scanning range of the PAA. This special radome will provide many potential applications in the future.

We can use the metric matching method [14, 16] to analyze the reflection problems of our radome. At the output surface of our cylindrical radome described by Eq. (6), the basis vectors in the reference and real space are ($\hat{e}_r$, $\hat{e}_\theta$, $\hat{e}_z$) and $(\hat{e}_{r'}, \hat{e}_{\theta'}, \hat{e}_{z'}) = (\hat{e}_r, M\hat{e}_\theta + \frac{R_2}{R_2-R_1}[(M-1)\theta' - M\theta_0]\hat{e}_r, \hat{e}_z)$ respectively. The metric matching condition $\hat{e}_i\cdot\hat{e}_{i'} = 1$, $i = r$, θ, z is satisfied for an angle shifter ($M = 1$ and $\theta_0 \neq 0$) in Figs. 2(d)–(f), and thus there is no reflection problem for the angle shifter. However, for an angle compressor ($M \neq 1$ and $\theta_0 = 0$) in Figs. 2(g)–(i), the metric matching condition is not satisfied, and thus there exists a reflection which will reduce the gain of the antenna system. To extend the scanning angle of a PAA, an angle shifter can be utilized without any reflection problem (i.e., without reducing the gain of the antenna system).

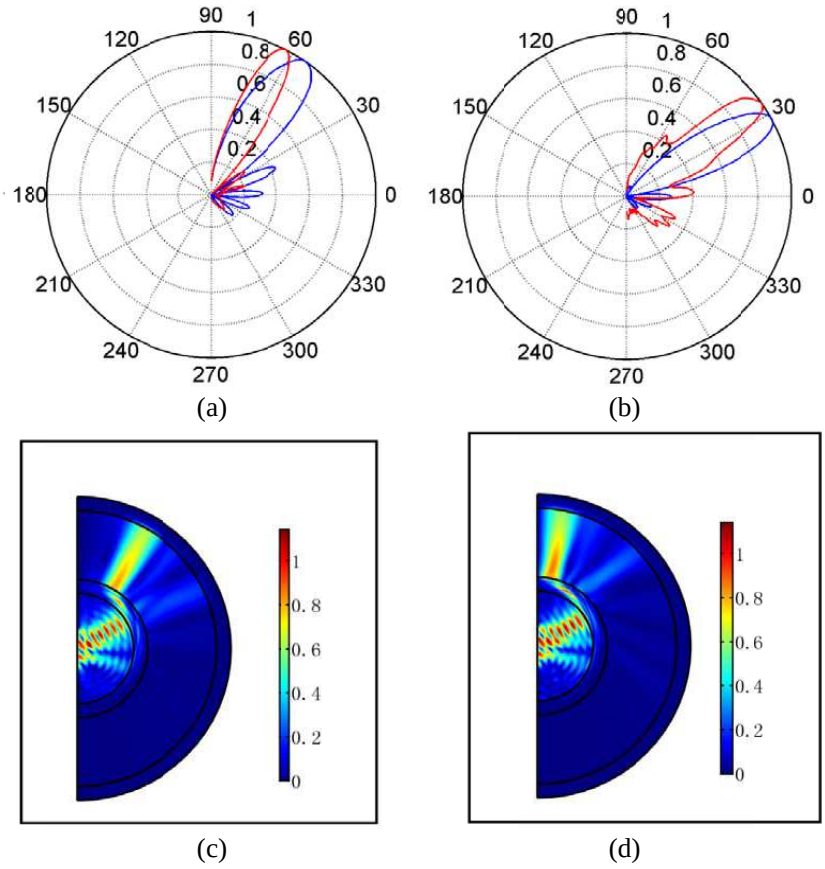

Figure 3. The normalized amplitude of electric far field. (a) We use a PAA to produce a beam with angle 65° (blue line) and use a radome with $\theta_0 = 45°$ and $M = 1$ (an angle shifter) after a beam with angle 20° is produced by a PAA (red line). The PAA is chosen to be the same as in Fig. 2. If we combine a PAA with our radome used for an angle shifter, we can achieve an output beam with angle 65° (keeping good directivity and low side lobe) in the far field. (b) We use a PAA to produce a beam with angle 30° and use a radome with $\theta_0 = 0$ and $M = 2$ (an angle compressor) after a beam with angle 60° is produced by a PAA (red line). (c) and (d) are amplitudes of the electric field distribution when a beam with angle 30° produced by the PAA is incident onto our radome. (c) We produce an output beam with an angle of 60° and a smaller width by using a multi-functional radome with $\theta_0 = 45°$ and $M = 2$. (d) We produce an output beam with an angle of 80° and a smaller width by using a multi-functional radome with $\theta_0 = 65°$ and $M = 2$.

3. DESIGNING AN ARBITRARY SHAPED RADOME

In this section, we will present a general method for designing a radome of arbitrary shape. In practical applications, radomes of various shapes are required for different occasions. Traditional FET is often applied on a slab-shaped region where Γ_1 and Γ_2 are two infinitely long straight lines parallel to the y' axis. Here we will extend FET to an arbitrary region enclosed by Γ_1, Γ_2 and y' axis. Inspired from the method of designing a cloak of arbitrary shape [18], we can let the inner and outer boundary of our radome (Γ_1 and Γ_2) be of arbitrary shape (see Fig. 1). To form a radome with the function described in Eq. (3), we need to find a continuous function f that satisfies the boundary condition described by Eq. (2). There may be countless possible continuous functions f, and we can acquire one of these functions by solving the Laplace equation under this boundary condition (Eq. (2)). For convenience of solving the Laplace equation, we first extend the boundaries Γ_1 and Γ_2 to form an enclosed region (see Fig. 4) by mirror transformation Γ_1 and Γ_2 on the y axis. We can then solve the Laplace equation on

this enclosed domain with the boundary condition described by Eq. (2). After we find the continuous function f and the transformed materials, we can simple drop the region $x' < 0$ and keep the region $x' > 0$ as our radome. When Γ_1 and Γ_2 are arbitrarily shaped boundaries, it is more convenient to solve this problem in the Cartesian coordinate system. We can rewrite the transformation relation Eq. (1) in the following form:

$$\begin{aligned} x &= f_1\left(x', y'\right) \\ y &= f_2\left(x', y'\right) \\ z &= z' \end{aligned} \tag{11}$$

Boundary condition (2) can also be expressed in Cartesian coordinates:

$$\begin{aligned} f_1|_{\Gamma_1} &= x'; \quad f_1|_{\Gamma_2} = x'\cos\Delta\theta + y'\sin\Delta\theta \\ f_2|_{\Gamma_1} &= y'; \quad f_2|_{\Gamma_2} = -x'\sin\Delta\theta + y'\cos\Delta\theta \end{aligned} \tag{12}$$

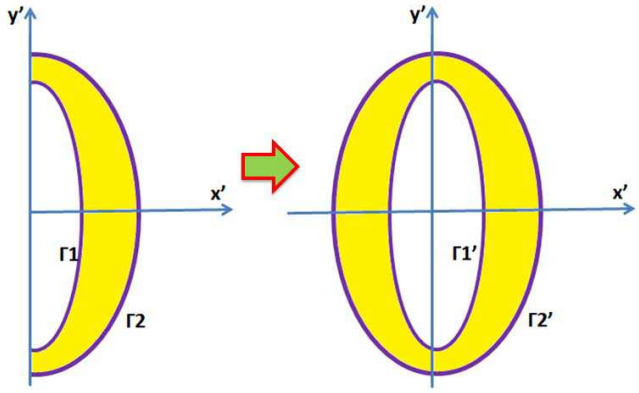

Figure 4. The method to design an arbitrarily shaped radome. For convenience in solving the Laplace equation, we first extend the boundaries Γ_1 and Γ_2 to Γ_1' and Γ_2' by a mirror transformation on the y'-axis. We can solve the Laplace equation in the region enclosed by Γ_1' and Γ_2'. After we get the solution of the Laplace equation, the transformed materials can be calculated. We can simply leave the transformed materials in the region $x' > 0$ as our radome, which is the same region enclosed by boundaries Γ_1, Γ_2 and the y-axis.

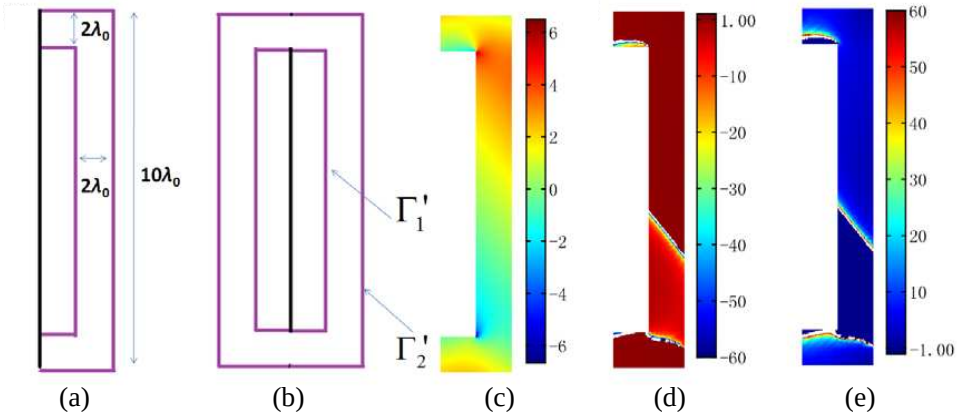

Figure 5. (a) A rectangular radome. Purple lines indicate the boundaries of the radome. (b) To solve the Laplace equation, we need to extend the boundaries as we have explained in Fig. 4. (c) The z-component of the calculated permittivity (for TE model). (d) and (e) Two principal values of the calculated permeability tensor in the x'-y' plane. Some small white regions in (d) and (e) indicate that the value is beyond the color bar.

with

$$\Delta\theta = \theta_{output} - \theta_{input} = G^{-1}(\theta_{input}) - \theta_{input} \tag{13}$$

Next we demonstrate our method with an example. As a slab-shaped structure is easy to fabricate, we first design a rectangularly shaped radome and later extend it to a slab-shaped one. The size of the radome is shown in Fig. 5(a). As we have mentioned before, we first extend the shape of our radome to another enclosed shape for convenience to solve the boundary problem (see Fig. 5(b)). Note that we do not analyze the case of complex relation between the input and output angle in this paper. [In practical applications, a linear relation (but not a complex one) is often desired. In addition, the more complex the relation between θ_{input} and θ_{output}, the more likely discontinuous transformation at the output boundary of the device. Similarly to other devices designed by FET, this means that the reflection at the output boundary will be more serious, which may greatly degrade the performance of the device.]. The desired relation between the input angle and the output angle now is still chosen to be a linear relationship by Eq. (5) with $M = 1$ and $\theta_0 = 45°$. In this case we can obtain $\Delta\theta = \theta_0 = 45°$ in Eq. (12). By solving Laplace equations $(\partial^2_{x'} + \partial^2_{y'})f_1 = 0$ and $(\partial^2_{x'} + \partial^2_{y'})f_2 = 0$ with boundary condition (12) with $\Delta\theta = 45°$, we can obtain numerically the continuous transformation functions f_1 and f_2 in Eq. (11). Then the permittivity and permeability of the transformed medium can be determined (see Figs. 5(c)–(e)) by using TO [18].

We use FEM to simulate the performance of the designed radome of rectangular shape in Fig. 5.

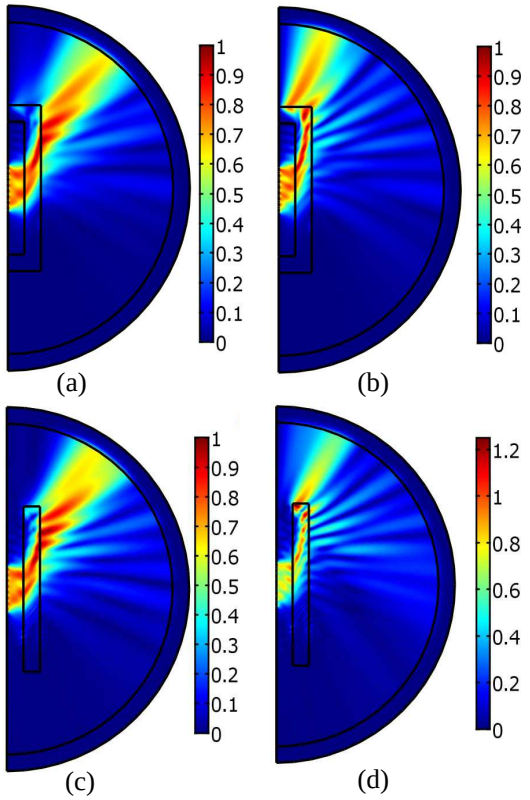

Figure 6. 2D FEM simulation results: the amplitude of the electric field distribution. The size of the whole simulation domain is the same as the one in Fig. 2. The TE model (where the electric field is orthogonal to the x'-y' plane) is simulated here. An 8×1 PAA, which is the array of line segments with equal length $0.25\lambda_0$ and center-to-center spacing $d = 0.35\lambda_0$, is set along the PEC ground (y'-axis). (a) and (b) we set a rectangular radome in Fig. 4 above the PAA (the incident angle is 10° and 30°, respectively). (c) and (d) we set a slab-shaped radome (we simply cut off the two arms of the rectangular radome in (a) to obtain this slab-shaped radome) above the PAA (the incident angle is 10° and 30°, respectively).

As shown in Figs. 6(a) and (b), our radome performs very well. We also simulate the performance of a slab-shaped radome that is simply cut from the rectangular one (see Figs. 6(c) and (d)). The numerical simulation shows that such a slab-shaped radome still performs well on steering the angle of a PAA. The slab radome in Figs. 6(c) and 6(d) have been simplified by cutting off the two arms of the rectangular radome in Fig. 6(a). More unwanted side-lobes appear due to such a simplification and scattering at a sharp corner of the slab.

4. SUMMARY AND DISCUSSION

In this paper, we first propose a general method on how to use the FET to design some non-slab shaped devices. Two specific shaped radomes that can extend the scanning angel of a PAA have been designed. The FEM simulation results suggest good performance of our device. Compared with previous radomes, our radome has the following advantages: firstly the relation between the incident angle produced by a PAA and the steered output angle by our radome can be manipulated as necessary (e.g., a linear relation can be achieved). Secondly, the shape of the radome can also be designed arbitrarily for different applications. In addition, our method does not require any optimization process compared to other methods which requires massive optimization.

Although the examples shown in this paper are 2D structures, extending our 2D design to 3D one is fairly straightforward. There is still more work to be done, however, if we want to realize our radome in practice. As we can see from Eq. (8), the realization of this device requires inhomogeneous, magnetic and anisotropic materials, which can be realized by meta-materials. Before we realize it, we need to do some simplification as how people constructed the invisibility cloaking. Another possible way to simplify the material requirement of the proposed radome is to choose some other kinds of transformation function. Note that there are many continuous function f which satisfies the boundary condition (5), and here we just choose the simplest linear transformation function of Eq. (4) to demonstrate our idea. Our subsequent work is simplifying the material parameters of our radome or finding some other transformation function that can achieve a less demanding material requirement.

ACKNOWLEDGMENT

This work is partially supported by the National High Technology Research and Development Program (863 Program) of China (No. 2012AA030402), the National Natural Science Foundation of China (Nos. 61178062 and 60990322), the Program of Zhejiang Leading Team of Science and Technology Innovation, Swedish VR grant (# 621-2011-4620) and SOARD. Fei Sun thanks the China Scholarship Council (CSC) No. 201206320083.

REFERENCES

1. Mailloux, R. J., *Phased Array Antenna Handbook,* 2nd edtion, Artech House, Boston, MA, 2005.
2. Lam, T. A., C. G. Parazzoli, and M. H. Tanielian, "Negative index metamaterial lens for the scanning angle enhancement of phased array antennas," *Metamaterials and Plasmonics: Fundamentals, Modeling, Applications*, S. Zouhdi, A. Sihvola, and A. Vinogradov (eds.), 121–138, Springer-Verlag, New York, 2008.
3. Lam, T. A., D. C. Vier, J. A. Nielsen, C. G. Parazzoli, and M. H. Tanielian, "Steering phased array antenna beams to the horizon using a buckyball NIM lens," *Proceedings of IEEE*, Vol. 99, No. 10, 1755–1767, 2011.
4. Leonhardt, U. and T. G. Philbin, *Geometry and Light: Science of Invisibility*, Dover, 2010.
5. Pendry, J. B., D. Schurig, and D. R. Smith, "Controlling electromagnetic fields," *Science*, Vol. 312, No. 5781, 1780–1782, 2006.
6. Pendry, J. B., "Negative refraction makes a perfect lens," *Phy. Rev. Lett.*, Vol. 85, 3966, 2000.
7. Sun, F. and S. He, "Create a uniform static magnetic field over 50 T in a large free space region," *Progress In Electromagnetics Research*, Vol. 137, 149–157, 2013.

8. Sun, F. and S. He, "DC magnetic concentrator and omnidirectional cascaded cloak by using only one or two homogeneous anisotropic materials of positive permeability," *Progress In Electromagnetics Research*, Vol. 142, 683–699, 2013.
9. Sun, F. and S. He, "Novel magnetic lens for static magnetic field enhancement," *PIERS Proceedings*, 1689–1691, Stockholm, Sweden, Aug. 12–15, 2013.
10. Sun, F. and S. He, "Static magnetic field concentration and enhancement using magnetic materials with positive permeability," *Progress In Electromagnetics Research*, Vol. 142, 579–590, 2013.
11. Chen, H., C. T. Chan, and P. Sheng, "Transformation optics and metamaterials," *Nature Materials*, Vol. 9, No. 5, 387–396, 2010.
12. Rahm, M., D. Schurig, D. A. Roberts, S. A. Cummer, D. R. Smith, and J. B. Pendry, "Design of electromagnetic cloaks and concentrators using form-invariant coordinate transformations of Maxwell's equations," *Photonics Nanostruct. Fundam. Appl.*, Vol. 6, 87–95, 2008.
13. Chen, H. and C. T. Chan, "Transformation media that rotate electromagnetic fields," *Appl. Phys. Lett.*, Vol. 90, 241105–241105, 2007.
14. Rahm, M., S. A. Cummer, D. Schurig, J. B. Pendry, and D. R. Smith, "Optical design of reflectionless complex media by finite embedded coordinate transformations," *Phys. Rev. Lett.*, Vol. 100, 063903, 2008.
15. García-Meca, C., M. M. Tung, J. V. Galán, R. Ortuño, F. J. Rodríguez-Fortuño, J. Martí, and A. Martínez, "Squeezing and expanding light without reflections via transformation optics," *Opt. Express*, Vol. 19, No. 4, 3562–3575, 2011.
16. Kwon, D. H. and D. H. Werner, "Polarization splitter and polarization rotator designs based on transformation optics," *Opt. Express*, Vol. 16, No. 23, 18731–18738, 2008.
17. "The finite element simulation is conducted by using commercial software COMSOL Multiphysics," http://www.comsol.com/.
18. Hu, J., X. Zhou, and G. Hu, "Design method for electromagnetic cloak with arbitrary shapes based on Laplace's equation," *Opt. Express*, Vol. 17, 1308–1320, 2009.
19. Amitay, N., V. Galindo, and C. P. Wu, *Theory and Analysis of Phased Array Antennas*, Wiley-Interscience, 1972.